Conference on Modelling Fluid Flow (CMFF'25)
The 19th International Conference on Fluid Flow Technologies
Budapest, Hungary, August 26-August 29, 2025

Investigation of Radius Ratio Effects on Velocity Statistics in Annular Pipe Flow using One-Dimensional Turbulence

Pei-Yun Tsai[1,2,3], Li Toong Yap[2,3], Marten Klein[2,3], Heiko Schmidt[2,3]

[1] Corresponding Author. Tel.: +49 (0) 355 69 5127, Fax: +49 (0) 355 69 4891, E-mail: tsaipeiy@b-tu.de
[2] Chair of Numerical Fluid and Gas Dynamics, Faculty of Mechanical Engineering, Electrical and Energy Systems, Brandenburg University of Technology Cottbus-Senftenberg. Siemens-Halske-Ring 15A, 03046 Cottbus, Germany
[3] Scientific Computing Lab, Energy Innovation Center, Brandenburg University of Technology Cottbus-Senftenberg. Universitätsstraße 22, 03046 Cottbus, Germany

ABSTRACT

Concentric coaxial (annular) pipe flows are numerically investigated using a stochastic one-dimensional turbulence (ODT) model. ODT offers full-scale resolution of the radial boundary layers and their dynamical variability. Based on the latter, it is demonstrated for various Reynolds numbers that spanwise wall-curvature affects low-order and detailed velocity statistics. Wall curvature leads to radial asymmetry in the flow statistics, limiting the applicability of conventional wall-function models that assume a universal von Kármán constant and a locally flat surface. Resolving the near-wall turbulence is essential for predictive capabilities, but a computational burden that is addressed by the dimensionally reduced modeling within ODT. The model is able to reproduce and predict consistent low-order and detailed turbulence statistics. By utilizing boundary-layer theory, it is shown how the model can be used to obtain curvature-aware velocity wall function, which is of broader relevance for modeling engineering applications such as coaxial heat exchangers.

Keywords: annular pipe flow, spanwise wall curvature, stochastic modeling, turbulence statistics, turbulent boundary layer

NOMENCLATURE

$\mathcal{E}$	$[-]$	Eddy event
D^+	$[-]$	Parametrization coefficient
P	$[Pa]$	Pressure
R_i, R_o	$[m]$	Radius of inner and outer cylinders, respectively
Re_b	$[-]$	Bulk Reynolds number: $4\overline{u}_b\delta/\nu$
$Re_{\tau i}$, $Re_{\tau o}$	$[-]$	Friction Reynolds number at inner and outer walls: $u_{\tau,i}\delta/\nu$, $u_{\tau,o}\delta/\nu$
β^+	$[-]$	Parametrization coefficient
δ	$[m]$	Half width of the gap between inner and outer pipe walls: $(R_o - R_i)/2$
$\delta(\cdot)$	$[-]$	Dirac distribution function
δ_ν	$[-]$	Viscous length scale: ν/u_τ
η	$[-]$	Radius ratio: R_i/R_o
ν	$[m^2/s]$	Kinematic viscosity
ρ	$[kg/m^3]$	Mass density of fluid
r_m	$[m]$	Radial location of maximum mean axial velocity occurs
t	$[s]$	Time
t_e	$[s]$	Sampled times of eddy event
$\overline{u}_b$	$[m/s]$	Bulk mean velocity
τ_{wi}, τ_{wo}	$[N/s^2]$	Mean wall shear stress on the inner and outer walls, respectively
$u_{\tau i}$, $u_{\tau o}$	$[m/s]$	Wall friction velocity at inner and outer walls : $\sqrt{\tau_{wi}/\rho}$, $\sqrt{\tau_{wo}/\rho}$

Subscripts and Superscripts

DNS	Direct numerical simulation
ODT	One-dimensional turbulence
PDF	Probability density function
RSS	Reynolds shear stress
u, v, w	Velocity component in the x, r, θ direction, respectively
x, r, θ	Coordinates of the axial, radial, and azimuthal directions, respectively
$\overline{(\cdot)}$	Temporal mean
$(\cdot)^+$	Wall coordinate
$(\cdot)'$	Fluctuating component
$(\cdot)_i$, $(\cdot)_o$	Values at the inner and outer walls, respectively
$(\cdot)_{max}$	Maximum value
$(\cdot)_{rms}$	Root-mean-square value

1. INTRODUCTION

Annular pipe flow is found in various engineering applications, such as coaxial geothermal heat ex-

changers, photochemical reactors, and gas-cleaning devices. The investigation of turbulent annular pipe flow is a canonical problem that provides detailed insights into radial transport processes and boundary layers over both convex and concave walls. Unlike turbulent channel flow, the presence of curved surfaces leads to a closure problem, as the inner and outer pipe wall contributions to skin friction drag and pressure loss are undetermined and differ from each other, resulting in a simulation result [1]. This circumstance needs to be addressed with predictive modeling capabilities.

In recent decades, numerous numerical and experimental studies have been carried out to better understand the characteristics of pressure-driven (Poiseuille) turbulent flow in concentric annular pipes. In the last century, a major debate centered on whether the location of maximum radial velocity coincides with the point of zero shear stress. Several experimental studies were conducted on this topic [2, 3]. Chung et al. [4] performed the first comprehensive DNS study of turbulent annular pipe flow at a fixed bulk Reynolds number $Re_b = 8900$, analyzing the effect of spanwise curvature in turbulent properties for two radius ratios, $\eta = R_i/R_o = 0.1$ and 0.5, where R_i (R_o) denotes the radius of the inner (outer) pipe as sketched in Fig. 1 below. Here, the bulk Reynolds number is defined as $Re_b = 4\overline{u}_b\delta/\nu$, with $\overline{u}_b$ representing the bulk mean velocity, $\delta = (R_o - R_i)/2$, and ν being the kinematic viscosity of the fluid. Boersma and Breugem [1] studied turbulent flow in an annular pipe using DNS at a small radius ratio ($\eta \leq 0.1$) over a moderate range of Reynolds numbers. More recently, Bagheri and Wang [5] conducted a DNS study to examine the effects of radius ratio on turbulent statistics and structures in both physical and spectral spaces across multiple radius ratio cases ($eta = 0.1, 0.3, 0.5,$ and 0.7). As an extension, turbulent heat transfer in the annular pipe flow, coupled with passive scalar, has also been discussed [6, 7].

Despite the efforts described above, a theoretical justification of empirical pressure loss properties has remained elusive, as the boundary layer near the curved inner wall is virtually inaccessible to measurement. Furthermore, high-fidelity numerical simulations have high-resolution requirements [1] such that high Reynolds numbers have not been assessed until recently for wide annular gaps [8, 9]. Klein et al. [9] conducted annular pipe flow simulations using the conventional LES-WALE model and found that this approach may not be ideal for accurately capturing small-scale flow physics near curved walls. The objective of this study is to pave the way toward the development of improved wall functions applicable to spanwise curved walls for utilization in classical large-eddy and Reynolds-averaged simulations. This is achieved by adopting an alternative approach that utilizes Kerstein's one-dimensional turbulence (ODT) model [10, 11], which evolves instantaneous boundary layer profiles. The model extension to cylindrical geometry [12], calibrated for annular pipe flow [13], is utilized here as a stand-alone tool. The model formulation and mesh-adaptive implementation provide full-scale resolution of the instantaneous radial profiles of the velocity vector across the annular gap. Dimensional model reduction offers major cost reduction, making high Reynolds number cases feasible.

The rest of this paper is organized as follows. Section 2 gives some details of the annular pipe flow setup investigated. Section 3 provides an overview of the ODT model formulation and the governing equations. Section 4 discusses the main results in terms of velocity statistics, focusing on examining the impact of spanwise curvature on some turbulence properties. Last, section 6 summarizes the key findings of this work.

2. ANNULAR PIPE FLOW

An incompressible, constant-property Poiseuille flow confined between two concentric coaxial cylinders is considered, as sketched in Fig. 1. No-slip boundary conditions are prescribed at the pipe walls, and an axial mean pressure gradient force is applied to drive the flow. The numerical domain of the stochastic ODT simulations (ODT domain) represents a single radial coordinate spanning the entire gap between the cylinders.

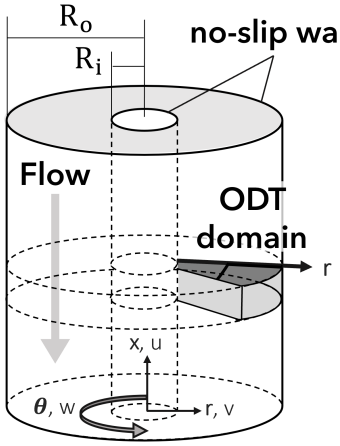

Figure 1. Schematic of the annular pipe flow configuration investigated. The wedge-shaped, radially oriented ODT domain is exaggerated. No-slip boundary conditions are prescribed at the walls as indicated.

3. NUMERICAL MODEL

3.1. ODT Model Formulation

In the ODT model, the conservation equations are dimensionally reduced and solved numerically by representing turbulent advection as a stochastic process. The flow in axial and azimuthal directions is assumed to be statistically homogeneous. This process employs instantaneous spatial mapping events that

intermittently modify the deterministic flow evolution. Following [12] and applying the notation from [14], the dimensionally reduced ODT equations for temporally evolving flow are given by

$$\frac{\partial u_i}{\partial t} + \sum_{t_e} \mathcal{E}_i \, \delta\left(t - t_e\right) = \frac{1}{r}\frac{\partial}{\partial r}\left(r\nu\frac{\partial u_i}{\partial r}\right) - \frac{1}{\rho}\frac{\mathrm{d}P}{\mathrm{d}x}\,\delta_{ix} \; . \tag{1}$$

Here, u_i, $i = x, r, \theta$, represents the model-resolved instantaneous velocity vector with cylindrical components $u_x = u$, $u_r = v$, $u_\theta = w$, corresponding to the axial, radial, and azimuthal directions, respectively. t indicates the time, t_e the stochastically sampled times of eddy event $\mathcal{E}_i$ ($i = x, r, \theta$) occurrences, $\delta(t)$ the Dirac distribution function. $\mathrm{d}P/\mathrm{d}x$ denotes the prescribed mean pressure-gradient force in the axial direction, δ_{ij} the Kronecker delta, ν the kinematic viscosity, and ρ the mass density of the fluid.

ODT utilizes map-based advection modeling [10] to represent instantaneous modifications to the flow profile associated with the turnover of a notional eddy. In this study, the generalized baker's map denoted "triplet map B" (TMB) [12] is specifically used, as it ensures scale-locality, equidistant fluid parcel displacement, and adheres to physical conservation principles for radial transport. Further details on the formulation of the eddy events $\mathcal{E}_i$ and the cylindrical mapping techniques can be found in [12, 14]. The calibration of ODT model parameters for turbulent annular pipe flow is thoroughly discussed in [13, 8] and is not repeated here.

3.2. Grid Sensitivity Analysis

The radially oriented ODT domain is discretized using an adaptive grid, capable of resolving all relevant scales of the flow locally. The grid must be fine enough to resolve the viscous sublayer and the smallest emerging features at and off the wall in the evolving transient solution. To ensure that the results are independent of the grid resolution and that numerically, mesh-adaptive transport is negligible, a grid sensitivity study was conducted.

Table 1 presents the ODT test cases with varying grid resolutions. Case A represents the resolution used throughout this study. Case B uses a finer grid, with half the grid size of Case A; Case C employs a medium resolution with double the grid size of Case A; and Case D corresponds to a coarser resolution, with four times the grid size of Case A. The parameters Δr_min and Δr_max denote the minimum and maximum grid cell sizes in the ODT model, respectively, keeping the adaptivity range constant at $\Delta r_\mathrm{max}/\Delta r_\mathrm{min} = 20$. The difference in friction Reynolds number between Case A and the finer Case B is found to be less than 0.1%. Compared to the reference DNS data from [4], where $Re_{\tau i} = 179$ and $Re_{\tau o} = 141$, Case A achieves excellent agreement, with deviations of less than 0.1% at both the inner and outer walls. This confirms that Case A provides a sufficiently effective resolution to ensure accurate predictions of near-wall small-scale physics. Additionally, since ODT does not involve multi-dimensional mesh geometry, traditional grid quality metrics, such as skewness and aspect ratio, are not applicable in this modeling framework.

Table 1. Friction Reynolds numbers at the inner and outer walls for different grid resolutions. Case A corresponds to the resolution used for all simulations in this study, while the other three cases (B, C, and D) are included for grid resolution testing and comparison.

Cases	Δr_{min}	Δr_{max}	$Re_{\tau i}$	$Re_{\tau o}$
A	$\delta/1000$	$\delta/24$	179.12	144.46
B	$\delta/2000$	$\delta/48$	179.24	144.69
C	$\delta/500$	$\delta/12$	182.73	144.56
D	$\delta/250$	$\delta/6$	206.01	149.15

3.3. Statistical Convergence

The ODT model presents the simulation results in ensemble-averaged form over long simulation times. To ensure statistical stationarity, the data collection began after a warm-up phase that was estimated by short presimulations.

To assess statistical convergence, mean axial velocity profiles from two test cases with different numbers of generated eddy events (N_eddy) are shown in Fig. 2. On average, the model generates approximately three eddy events per second of wall-clock time. The case with 4400 eddy events is shown to be sufficiently qualified to reproduce the mean profile of the reference DNS. In practice, all simulations used in this study were run for a sufficient duration to generate an adequate number of eddy events such that second-order statistical moments converged in a similar manner. These results confirm the robustness of the reported statistics with respect to both random initialization and simulation duration, indicating that the simulations have achieved statistical convergence.

4. RESULTS AND DISCUSSION

4.1. Mean Velocity Profile

Fig. 3 compares the mean axial velocity profiles with the DNS data [4]. Mean velocity is normalized by bulk mean velocity $\overline{u}_b$. An excellent agreement is observed between the ODT results and DNS data for radius ratio $\eta = 0.1$ and 0.5 with fixed bulk Reynolds number $Re_b = 8900$, that the boundary layer radial asymmetry is correctly represented. The asymmetry results in the development of a thicker boundary layer over the outer cylinder surface compared to the inner cylinder surface. This is more pronounced in the radius ratio $\eta = 0.1$ case than $\eta = 0.5$ case.

The influence of wall curvature is noticeably stronger near the inner pipe wall than at the outer pipe wall. This effect becomes even more significant

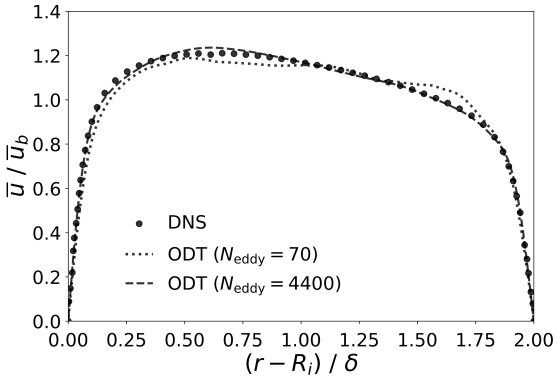

Figure 2. Comparison of two ODT axial mean velocity profiles, normalized by $\overline{u}_b$, at $\eta = 0.1$ and $Re_b = 8900$, after accumulation of $N_{\text{eddy}} = 700$ and 4400 implemented stochastic eddy events, respectively. Reference DNS data is from [4].

in smaller radius ratios, where the velocity gradient at the inner pipe wall is steeper. The dotted vertical lines in Fig. 3 represent the calculated location of the maximum mean axial velocity $\overline{u}_{max}$ determined using the Kays–Leung relation, which has been experimentally validated [3]. The location r_m, where the maximum mean axial velocity occurred, depends on the radius ratio of the inner and outer pipes and is parameterized as

$$\frac{r_m - R_i}{R_o - r_m} = \left(\frac{R_i}{R_o}\right)^{0.343} \quad . \tag{2}$$

A quantitative comparison of r_m as predicted by ODT to the Kays–Leung relation yields an error of less than 0.5. This is remarkable, considering the simplicity of the ODT model, and demonstrates that the map-based stochastic modeling approach effectively captures large-scale mixing-length effects.

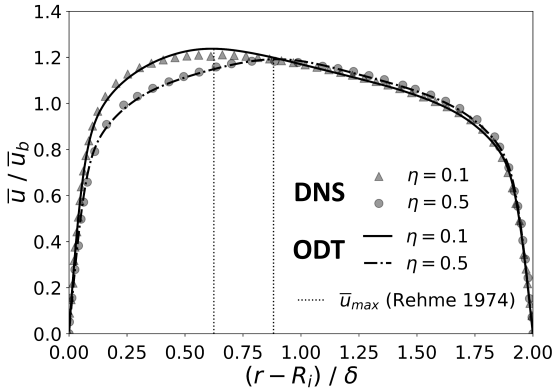

Figure 3. Radial profiles of the mean velocity $\overline{u}$ normalized with the bulk velocity $\overline{u}_b$ for radius ratio $\eta = 0.1$ and 0.5, respectively. The bulk Reynolds number is $Re_b = 8900$. Reference DNS data is from [4].

4.2. Velocity Boundary Layer

Fig. 4 extends the comparison from mean velocity profiles to the logarithmic velocity profiles. For the normalization purpose, the local friction velocities at the inner and outer walls are defined as

$$u_{\tau i} = \sqrt{\nu \left|\frac{\mathrm{d}u}{\mathrm{d}r}\right|_{wall,i}} \quad , \quad u_{\tau o} = \sqrt{\nu \left|\frac{\mathrm{d}u}{\mathrm{d}r}\right|_{wall,o}} \quad , \tag{3}$$

where $u_{\tau i}$ and $u_{\tau o}$ denote the friction velocity on the inner and outer pipe walls, respectively. The normalized mean velocity is defined as $u^+ = u/u_{\tau,o/i}$ and the corresponding radius as $r^+ = |r - R_{o/i}|\, u_{\tau,o/i}/\nu$. The friction Reynolds numbers are defined as $Re_{\tau i} = u_{\tau i}\delta/\nu$ and $Re_{\tau o} = u_{\tau o}\delta/\nu$ at the inner and outer walls, respectively.

Fig. 4(*top*) shows the velocity boundary layer profiles at the inner and outer pipe walls for radius ratio $\eta = 0.5$. It is found that wall curvature does not significantly impact the inner and outer velocity boundary layer profiles in the radius ratio $\eta = 0.5$ case. Both normalized profiles align with the master profile, corresponding to the classical law-of-the-wall for pipe flow [15]. The linear viscous sublayer and logarithmic-law region are captured for radius ratio $\eta = 0.5$. However, this is not the case for radius ratio $\eta = 0.1$.

Fig. 4(*bottom*) exhibits the velocity boundary layer profiles at both sides of the pipe walls for radius ratio $\eta = 0.1$ compared with DNS data [4]. It is seen that the deviation between the inner and outer boundary layers is significant, and the law-of-the-wall profile cannot capture the behavior of the inner profile. This deviation is attributed to the effect of wall curvature, which results from the decrease in the inner cylinder radius. To quantify the effect, velocity boundary layer analysis is applied to the model results, using a similar approach as previously employed in [1]. Consequently, the boundary layer over the inner pipe wall is divided into a viscous-dominated region and a mixing-length-dominated region.

4.2.1. The viscous-dominated region

Assuming that the flow is fully developed, all flow statistics are invariant in the axial and azimuthal direction, so that only steady balance equations for the radial dependence of the statistical moments of the flow variables remain. Application of the Reynolds-averaging procedure to Eq. (1), rearranging, and integrating once over the radial coordinate r yields the shear stress balance equation as

$$\overline{u'v'} - \nu\frac{\partial u}{\partial r} = -\frac{r}{2}\frac{1}{\rho}\frac{\mathrm{d}P}{\mathrm{d}x} + \frac{C_1}{r} \quad , \tag{4}$$

$$C_1 = -\frac{1}{\rho}\frac{\tau_o R_i - \tau_i R_o}{R_i/R_o - R_o/R_i} \quad . \tag{5}$$

Here, C_1 is an integration constant determined by the flow solution and the wall-shear stresses. The

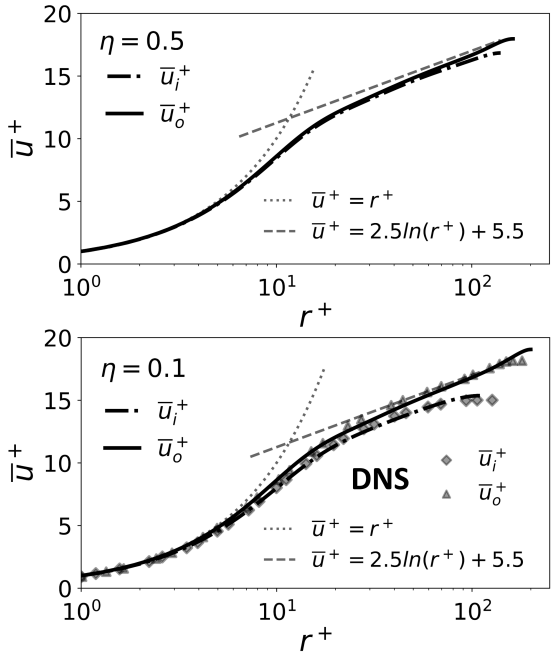

Figure 4. Velocity boundary layer at the inner $\overline{u_i}^+$ and outer $\overline{u_o}^+$ pipe wall, respectively, normalized by the local friction velocity for radius ratio $\eta = 0.1$ and 0.5 with fixed bulk Reynolds number $Re_b = 8900$.

term $\overline{u'v'}$ represents the ensemble effect of turbulent eddy events and serves as the model analog of the Reynolds stress [10, 14]. In the region very close to the wall, where $r < \delta_\nu$ (with the viscous length scale defined as $\delta_\nu = \nu/u_\tau$), it is assumed that the viscous stress dominates, meaning $\overline{u'v'} \ll \nu(\mathrm{d}u/\mathrm{d}r)$. For asymptotically small radius ratios, as $\eta \to 0$, Eq. (4) simplifies to

$$u_i^+(r^+) \approx R_i^+ \ln\left(\frac{r^+ + R_i^+}{R_i^+}\right) \quad , \tag{6}$$

where $R_i^+ = R_i\, u_{\tau,i}/\nu$ is not a constant but a parameter influenced by the wall geometry and the turbulent flow state. Specifically, it depends on the curvature radius and the wall-shear stress acting on the cylindrical inner wall. It is noted that, in this expression, the near-wall region deviates from the purely linear behavior described by the classical law of the wall and instead transitions to a logarithmic behavior.

4.2.2. The mixing-length-dominated region

In the mixing-length-dominated region, it is assumed that the total stress is primarily carried by the turbulent stress, such that $\nu(\mathrm{d}u/\mathrm{d}r) \ll \overline{u'v'}$. The influence of the radius is not negligible. For small asymptotic values of $\eta \to 0$, C_1 is simplified by assuming $R_o \gg R_i$, which retains radial information. Next, following [1], a conventional turbulent eddy viscosity ν_t parameterization is adopted. As suggested by [1], turbulent eddy viscosity can be expressed as $\nu_t = \beta\sqrt{\tau_i/\rho}\,(r - R_i)$, where β is an unknown proportionality factor that has to be estimated with data. Eq. (4) reduces to

$$u_i^+(r^+) \approx \frac{1}{\beta^+} \ln\left(\frac{r^+}{r^+ + R_i^+}\right) + D^+ \quad , \tag{7}$$

where β^+ and D^+ are parametrization coefficients that need to be determined with flow profile data.

Figure 5 presents the velocity boundary layer profiles at the inner pipe wall for three bulk Reynolds numbers ($Re_b = 8900$, 10^5, and 10^6), with the radius ratio fixed at $\eta = 0.1$. The profiles are validated using boundary layer theory. The corresponding values of the coefficients β^+ and D^+ for each case are summarized in Table 2. Based on these three test cases, empirical correlations for the coefficients β^+ and D^+ as functions of Re_b (at fixed $\eta = 0.1$) are proposed as: $\beta^+(Re_b) = 0.02\ln(Re_b) - 0.02$ and $D^+(Re_b) = 6.92Re_b^{0.1}$. These correlations serve as a preliminary model for characterizing the boundary layer behavior in annular pipe flow.

In the viscous-dominated region, Eq. (6) provides an accurate prediction of near-wall velocity profile, with a slightly extended validated length up to $r^+ \leq 10$, compared to the conventional linear wall expression. In the mixing-length-dominated region, Eq. (7) effectively captures the dominant statistical features of the turbulent boundary layer on the cylindrical inner wall across a range of Reynolds numbers. It is found that as the Reynolds number increases, a thicker boundary layer is found, and the curvature effect remains noticeable up to $Re_b = 10^6$.

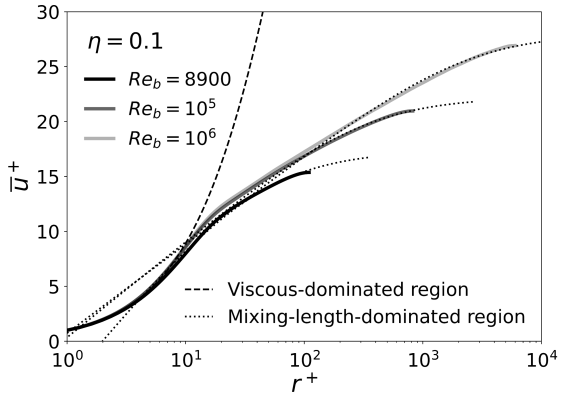

Figure 5. Velocity boundary layer at the inner pipe wall for various bulk Reynolds numbers $Re_b = 8900, 10^5, 10^6$ keeping the radius ratio $\eta = 0.1$ fixed.

Table 2. Coefficients in Eq. (7) for three test cases with fixed $\eta = 0.1$ varying the bulk Reynolds number.

Re_b	8900	10^5	10^6
β^+	0.1756	0.2617	0.2841
D^+	17.34	22.21	27.99

4.3. Reynolds Stress Components

Fig. 6 shows the Reynolds shear stress (RSS) $-\overline{u'v'}^+$ as a function of the wall-normal distance $(r - R_i)/\delta$ for radius ratio $\eta = 0.1$ and 0.5. The results show good agreement with the reference DNS data [5]. It is notable that the zero-crossing point for Reynolds shear stress (where $-\overline{u'v'}^+ = 0$) aligns with the location of the maximum mean axial velocity $\overline{u}_max$. This position is closer to the inner pipe wall for the minor radius ratio case, and the RSS profile becomes more symmetrical as the radius ratio increases. The difference in boundary layer thickness on the inner and outer pipe walls can also be clearly compared in this plot, as it is determined by the point where $-\overline{u'v'}^+ = 0$. This finding has already been discussed in Fig. 3. It is also observed that the magnitude of the RSS $-\overline{u'v'}^+$ is higher on the outer pipe wall than on the inner pipe wall, and this difference is more pronounced as the radius ratio decreases.

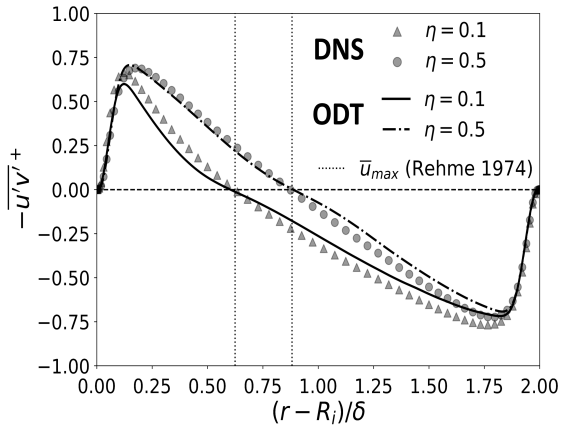

Figure 6. Radial profile of the Reynolds shear stress $-\overline{u'v'}^+$ for radius ratio $\eta = 0.1$ and 0.5, respectively, and fixed bulk Reynolds number $Re_b = 8900$. Reference DNS data is from [5].

Fig. 7 shows radial profiles of the axial component, $\overline{u'u'}^+$, of the normal Reynolds stresses in the vicinity of the inner and outer pipe walls with fixed radius ratio $\eta = 0.1$ and bulk Reynolds number $Re_b = 8900$ compared with reference DNS data [5]. Recall that $\overline{u'u'}^+ = (u_{rms}{}^+)^2$ is the variance or squared root-mean-square (RMS) axial velocity fluctuation. The axial velocity variance is a proxy for the turbulence intensity. The objective is to asses the model's capabilities to capture the radial asymmetry of velocity fluctuations across the gap. High $\overline{u'u'}^+$ value indicates the intense turbulence region. It is found that the maximum value of $\overline{u'u'}^+$ appears in the buffer layer, within the interval $5 < r^+ < 30$, which is in accord with the boundary layer over a flat surface. Compared to the profile of $\overline{u'u'}^+$ on the inner pipe wall, it is evident that the turbulence intensity on the outer pipe wall is stronger than on the inner pipe wall.

In contrast to the reference DNS data [5], ODT significantly underestimates the near-wall turbulent fluctuation peak at $r^+ \approx 15$, but it does capture the trend for the curvature influence. This behavior is consistent with the mean profiles discussed earlier, while underestimating turbulent fluctuations is a known modeling artifact [16, 12, 14]. The magnitude deficit of fluctuation and the underestimation of turbulence intensity do not necessarily imply incorrect radial fluxes. In fact, accurately capturing radial asymmetry requires a physical representation of radial fluxes in the dimensionally reduced model. As already shown in Fig. 6, this is achieved through map-based turbulence modeling within the eddy events, which are responsible for the advection of the radial velocity fluctuations, denoted as v'. It is also suggested that the ODT model may not be ideal for the low Reynolds number investigated. The model is primarily designed for highly turbulent flows, where no reference DNS data is available for turbulent annular pipe flow to support its application in this context. Therefore, the weaker turbulent fluctuations observed, in comparison to the DNS data, can be attributed to the effects of a finite Reynolds number. According to other ODT model studies [14], this type of modeling error tends to vanish for fluxes at high asymptotic Reynolds numbers. Therefore, based on the current model validation, the ODT model can be applied with greater confidence to heat exchangers, chemical reactors, and gas-cleaning devices that involve concentric pipe flows.

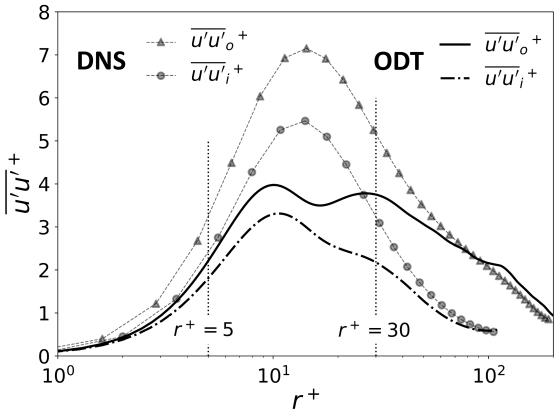

Figure 7. Radial profiles of the axial component of the Reynolds normal stresses in the vicinity of the inner and outer pipe wall, respectively, for bulk Reynolds number $Re_b = 8900$ and radius ratio $\eta = 0.1$.

4.4. Detailed Velocity Statistics

To better understand the variation in axial velocity fluctuation statistics with distance from the wall, the probability density function (PDF) of the fluctuating axial velocity is analyzed over the simulation time. Two distinct locations from both sides of the walls are selected: $r^+ = 5$ in the viscous-dominated

region and $r^+ = 30$ in the mixing-length-dominated region. From Fig. 7, it is known that at $r^+ = 30$, the difference of turbulent intensity between the outer and inner profiles is more extensive than at $r^+ = 5$.

Fig. 8 compares the PDF of the normalized fluctuating axial velocity u/u_{rms}, on the inner and outer pipe walls for two selected r^+ locations, with a radius ratio $\eta = 0.1$ and a bulk Reynolds number $Re_b = 8900$. The results indicate that the PDF curves generally exhibit a Gaussian-like distribution. However, as the location of r^+ changes, the peak of the PDF shifts toward higher magnitudes of u/u_{rms}, leading to a modification in the shape of the distribution profiles. It is seen that the shape of the profiles on the inner and outer pipe walls remains similar. Notably, at $r^+ = 30$, the difference in the magnitudes of u/u_{rms} between the inner and outer PDF profiles is more pronounced than at $r^+ = 5$. This indicates that the curvature effect on the fluctuating axial velocity is more significant at $r^+ = 30$ than at $r^+ = 5$. It is also observed that, compared to the PDF profile on the outer pipe wall, the magnitude of u/u_{rms} on the inner wall is generally higher, with the difference between each other becoming more pronounced as the distance from the pipe wall increases.

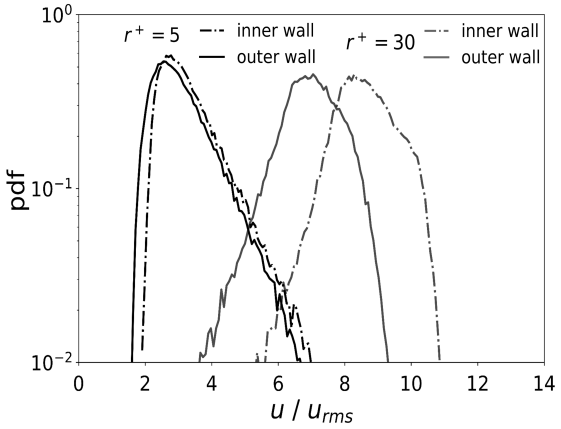

Figure 8. Probability density functions (PDFs) of the axial velocity fluctuations u normalized by the RMS u_{rms} at $r^+ = 5$ in the viscous sublayer and $r^+ = 100$ in the turbulent log layer on the inner and outer pipe walls for fixed radius ratio $\eta = 0.1$ and bulk Reynolds number $Re_b = 8900$.

5. UTILIZATION OF THE CURVATURE-AWARE WALL FUNCTION IN RANS

The application of the modified law-of-the-wall to predictive RANS-based modeling is demonstrated next. Equation 6 is applied as a wall function for the turbulent eddy viscosity in a 1-D finite-volume RANS solver using cylindrical coordinates (infinitesimal wedge). A mixing-length turbulence model with van Driest damping is used as a starting point, with the model coefficients obtained via fitting to DNS data from [4].

Figure 9 shows the mean velocity profile predicted by RANS using the modified wall function on the inner pipe wall in comparison to the reference DNS solution for $\eta = 0.1$ and $Re_b = 8900$. The two profiles are in close agreement, although the mean velocity on the inner pipe wall appears to be underestimated. Forthcoming research is devoted to evaluating the effectiveness of the spanwise curvature-aware wall function when utilized in multi-purpose CFD software.

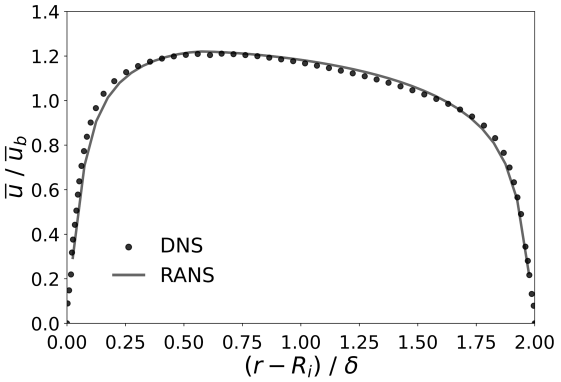

Figure 9. Comparison of RANS coupled with wall function from equation 6 with reference DNS data [4].

6. CONCLUSIONS

In the present study, stochastic one-dimensional turbulence (ODT) modeling of the pressure-driven flow in a concentric annular pipe has been presented and validated with available reference DNS.The stochastic model is formulated using the boundary-layer approximation. It can capture radial transport processes with full-scale resolution, even at high Reynolds numbers. The results demonstrate that the standalone ODT model offers a cost-effective approach to investigate statistical and dynamical features of fluctuating boundary layer flows.

For model validation, the profiles of mean velocity, law-of-the-wall on the inner and outer pipe walls, Reynolds shear stress, and axial Reynolds stress components are compared with reference DNS data [4, 5] at a fixed bulk Reynolds number of $Re_b = 8900$. Overall, the calibrated model reasonably reproduces low-order flow statistics. However, the model tends to underestimate axial velocity fluctuations, especially in the buffer layer, which is a well-known modeling artifact [16] that persists here at low radius ratios and high Reynolds numbers. Nevertheless, the model is able to capture fairly accurately the radial asymmetry and Reynolds shear stress distribution, which is a key asset for the present application.

It is observed that spanwise curvature affects the asymmetry of the mean velocity profile and, consequently, the thickness of the boundary layers on the inner and outer pipe walls. A lower radius ratio results in a thinner boundary layer on the inner

pipe wall. To enhance the wall-function-based prediction for the velocity boundary layer on the inner pipe wall, a theoretical analysis has been conducted, separately examining the viscous-dominated and mixing-length-dominated regions. By applying boundary-layer and mixing-length theories, the analysis successfully predicts the exact boundary layer profiles close to and farther away from the walls. This provides a reasonable basis for the development of curvature-aware wall functions as demonstrated by preliminary results for a low-Reynolds-number formulation.

ACKNOWLEDGEMENT

This research is supported by the German Federal Government, the Federal Ministry of Research, Technology and Space, and the State of Brandenburg within the framework of the joint project EIZ: Energy Innovation Center (project numbers 85056897 and 03SF0693A) with funds from the Structural Development Act for coal-mining regions.

REFERENCES

[1] Boersma, B. J., and Breugem, W.-P., 2011, "Numerical simulation of turbulent flow in concentric annuli", *Flow, Turbulence and Combustion*, Vol. 86 (1), pp. 113–127.

[2] Quarmby, A., 1967, "An experimental study of turbulent flow through concentric annuli", *International Journal of Mechanical Sciences*, Vol. 9 (4), pp. 205–221.

[3] Rehme, K., 1974, "Turbulent flow in smooth concentric annuli with small radius ratios", *Journal of Fluid Mechanics*, Vol. 64 (2), pp. 263–288.

[4] Chung, S. Y., Rhee, G. H., and Sung, H. J., 2002, "Direct numerical simulation of turbulent concentric annular pipe flow: Part 1: Flow field", *International Journal of Heat and Fluid Flow*, Vol. 23 (4), pp. 426–440.

[5] Bagheri, E., and Wang, B.-C., 2020, "Effects of radius ratio on turbulent concentric annular pipe flow and structures", *International Journal of Heat and Fluid Flow*, Vol. 86, p. 108725.

[6] Chung, S. Y., and Sung, H. J., 2003, "Direct numerical simulation of turbulent concentric annular pipe flow: Part 2: Heat transfer", *International Journal of Heat and Fluid Flow*, Vol. 24 (3), pp. 399–411.

[7] Bagheri, E., and Wang, B.-C., 2021, "Direct numerical simulation of turbulent heat transfer in concentric annular pipe flows", *Physics of Fluids*, Vol. 33 (5), p. 055131.

[8] Tsai, P.-Y., Schmidt, H., and Klein, M., 2023, "Investigating Reynolds number effects in turbulent concentric coaxial pipe flow using stochastic one-dimensional turbulence modeling", *Proceedings in Applied Mathematics and Mechanics*, Vol. 23 (4), p. e202300167.

[9] Klein, M., Tsai, P.-Y., and Schmidt, H., 2024, "Stochastic Modeling and Large-Eddy Simulation of Heated Concentric Coaxial Pipes", A. Dillmann, G. Heller, E. Krämer, C. Wagner, and J. Weiss (eds.), *New Results in Numerical and Experimental Fluid Mechanics XIV - Contributions to the 23rd STAB/DGLR Symposium Berlin, Germany 2022*, Springer, Vol. 154 of *Notes on Numerical Fluid Mechanics and Multidisciplinary Design*, pp. 435–444.

[10] Kerstein, A. R., 1999, "One-dimensional turbulence: model formulation and application to homogeneous turbulence, shear flows, and buoyant stratified flows", *Journal of Fluid Mechanics*, Vol. 392, pp. 277–334.

[11] Kerstein, A. R., Ashurst, W. T., Wunsch, S., and Nilsen, V., 2001, "One-dimensional turbulence: vector formulation and application to free shear flows", *Journal of Fluid Mechanics*, Vol. 447, pp. 85–109.

[12] Lignell, D. O., Lansinger, V. B., Medina, J., Klein, M., Kerstein, A. R., Schmidt, H., Fistler, M., and Oevermann, M., 2018, "One-dimensional turbulence modeling for cylindrical and spherical flows: model formulation and application", *Theoretical and Computational Fluid Dynamics*, Vol. 32 (4), pp. 495–520.

[13] Tsai, P.-Y., Schmidt, H., and Klein, M., 2023, "Modeling simultaneous momentum and passive scalar transfer in turbulent annular Poiseuille flow", *Proceedings in Applied Mathematics and Mechanics*, Vol. 22 (1), p. e202200272.

[14] Klein, M., Schmidt, H., and Lignell, D. O., 2022, "Stochastic modeling of surface scalar-flux fluctuations in turbulent channel flow using one-dimensional turbulence", *International Journal of Heat and Fluid Flow*, Vol. 93, p. 108889.

[15] Eggels, J. G., Unger, F., Weiss, M., Westerweel, J., Adrian, R. J., Friedrich, R., and Nieuwstadt, F. T., 1994, "Fully developed turbulent pipe flow: a comparison between direct numerical simulation and experiment", *Journal of Fluid Mechanics*, Vol. 268, pp. 175–210.

[16] Lignell, D., Kerstein, A., Sun, G., and Monson, E., 2013, "Mesh adaption for efficient multiscale implementation of one-dimensional turbulence", *Theoretical and Computational Fluid Dynamics*, Vol. 27, pp. 273–295.